IET Electrical Systems in Transportation

Special Issue: Energy Storage and Electric Power Sub-Systems for Advanced Vehicles (Based on IEEE-VPPC 2014)

IET Journals
The Institution of Engineering and Technology

Degraded mode operation of multi-stack fuel cell systems

ISSN 2042-9738
Received on 6th March 2015
Revised on 18th June 2015
Accepted on 12th August 2015
doi: 10.1049/iet-est.2015.0012
www.ietdl.org

Neigel Marx[1,2] ✉, David Camilo Toquica Cárdenas[1], Loïc Boulon[1], Frédéric Gustin[2], Daniel Hissel[2]

[1]*Institut de Recherche sur l'Hydrogène, Université du Québec à Trois-Rivières, Trois-Rivières, QC, Canada*
[2]*FCLAB, FR CNRS 3539, FEMTO-ST/Energy UMR CNRS 6174, University of Franche-Comte, Belfort, France*
✉ *E-mail: neigel.marx@uqtr.ca*

Abstract: Multi-stack fuel cell (MFC) systems provide higher performances and reliability than single-stack fuel cell systems through higher flexibility. The aim of this study is to investigate the degraded mode operation of MFC systems upon the loss of one of its stack. The different power allocation strategies impact the behaviour of the MFC system. Fuel consumption results obtained through simulation using a driving cycle acquired on a test vehicle are used to compare the chosen allocation strategies. The simulations have been conducted in a Matlab–Simulink environment. The results show that with a simple reconfiguration of the system the multi-stack system can still complete the driving cycle. The fuel consumption results during normal and degraded mode operation are compared and show acceptable efficiency loss during degraded mode operation.

Nomenclature

Roman symbols

A	free convection heat transfer surface (m^2)
A_t	forced convection heat transfer surface (m^2)
b_{11}	experimentally identified parameter
b_{12}	experimentally identified parameter
C_d	drag coefficient for the fan blades
C_{FC}	thermal capacity of the fuel cell stack ($J\ K^{-1}$)
E	electromotive force of the DC motor (V)
e_b	width of the fan blades (m)
E_c	activation energy of the reaction (66 $kJ\ mol^{-1}$)
E_n	Nernst potential (V)
F	faraday constant (96485 $A\ mol^{-1}$)
$\bar{h}$	average heat transfer coefficient ($W\ K^{-1}\ m^{-2}$)
ΔH	enthalpy of the reaction (W)
I_{conv}	current provided to the DC bus by the converter (A)
I_{FAN}	current provided to the DC motor (A)
I_{FC}	stack current (A)
I_{loss}	current representing the power loss in the converter (A)
j	current density ($A\ m^{-2}$)
j_0	exchange current density ($A\ m^{-2}$)
J_{FAN}	inertia of the fan axis + fan blades system ($kg\ m^2$)
j_L	current density limit ($A \cdot m^{-2}$)
j_{loss}	internal and fuel cross-over equivalent current density ($A\ m^{-2}$)
K	gain of the differential equation (18) (Ω)
K_1	fitting coefficient
K_2	fitting coefficient ($A\ cm^{-2}$)
K_3	fitting coefficient ($V\ K^{-1}$)
K_4	fitting coefficient (Ω cm^2)
K_5	fitting coefficient (K)
k_{aero}	mechanic–aerolic conversion coefficient for the fan blades
K_{purge}	state of purging valve
L_{conv}	inductance of the converter (H)
L_{FAN}	internal inductance of the DC motor (H)
N_b	number of blades
N_{cell}	number of cells
P_0	standard pressure (Pa)
P_{air}	air pressure in the cathodic chamber (Pa)
$P_{air,out}$	air pressure at the cathode outlet (Pa)
P_{O_2}	oxygen pressure in the cathodic chamber (Pa)
P_{H_2}	hydrogen pressure in the anodic chamber (Pa)
P_{H_2in}	pressure of the hydrogen flowing from the tank (Pa)
P_{H_2out}	pressure at the hydrogen outlet (Pa)
$q_{air,in}$	air flow at the cathode inlet ($m^3\ s^{-1}$)
$q_{air,fan}$	air flow expelled from V_{fan} by the fan ($m^3\ s^{-1}$)
$q_{air,out}$	air flow at the cathode outlet ($m^3\ s^{-1}$)
q_{conv}	convective heat transfer rate ($m^3\ s^{-1}$)
$q_{H_2,r}$	hydrogen flow consumed by the electrochemical reaction ($m^3\ s^{-1}$)
q_{H_2out}	hydrogen flow evacuated by the purge ($m^3\ s^{-1}$)
$q_{H_2}c$	hydrogen consumed by the fuel cell (reaction and purge) ($m^3\ s^{-1}$)
$q_{O_2,r}$	oxygen flow consumed by the electrochemical reaction ($m^3\ s^{-1}$)
$q_{H_2,in}$	Hydrogen flow flowing from the hydrogen tank ($m^3\ s^{-1}$)
R	universal gas constant (8, 314 $J\ K^{-1}\ mol^{-1}$)
R_0	starting radius of the fan blades (m)
R_{air}	hydraulic resistance between the inlet and outlet of the cathode (Pa s m^{-3})
R_b	radius of the fan blades (m)
R_{FAN}	internal resistance of the DC motor (Ω)
R_{H_2}	hydraulic resistance between the tank and the anode inlet (Pa s m^{-3})
R_m	membrane resistance (Ω)
R_{purge}	hydraulic resistance associated with hydrogen purge (Pa s m^{-3})
$\Delta S_{conv,Air}$	entropy exchange rate from the fuel cell to the air ($W\ K^{-1}$)
$\Delta S_{conv,FC}$	entropy exchange rate from the air to the fuel cell ($W\ K^{-1}$)
ΔS_q	heat generated by the electrochemical reaction
T_0	standard temperature (298,15 K)
T_{aero}	resistant torque created by drag forces on the fan blades (N m)
T_{air}	air temperature (K)
T_{FC}	mean fuel cell temperature (K)
T_m	torque provided by the DC motor (N m)
t_{mb}	membrane thickness (m)
T_{loss}	resistant torque composed of the magnetic and mechanic losses (N m)

U_{bus}	DC bus voltage (V)
U_{conv}	output voltage of the converter (V)
U_{FC}	voltage of the fuel cell stack (V)
ΔV_{act}	activation over-voltage (V)
ΔV_{conc}	concentration over-voltage (V)
ΔV_{mem}	dynamic over-voltage (V)
ΔV_{Ω}	ohmic losses (V)
V_{AN}	volume of the anodic chamber (m^3)
V_{cell}	cell voltage (V)
V_{mol}	volume of 1 mol of ideal gas (m^3)
V_{fan}	volume of the space between the fuel cell and the fan (m^3)
x_{O_2}	oxygen partial pressure (0.2095)

Greek symbols

α	duty cycle of the converter
η_{aero}	efficiency of the mechanic–aerolic conversion
η_{therm}	heat transfer efficiency
Λ_{mb}	membrane water content (14)
Ω	rotation speed of the DC motor (s^{-1})
τ	time constant of the differential equation (18) (s)
θ	pitch angle of the fan's blades (deg)
$\theta_{b,lm}$	log mean temperature difference of the air flow (K)

1 Introduction

Nowadays, fossil fuel powered vehicles are part of the issue behind climate change due to the greenhouse gas they emit. However, these vehicles are still more common than other alternatives in the transportation industry due to their low cost, high lifetime and high reliability. In this context, the zero emission vehicles require improvements especially on their autonomy and reliability. To this end, the use of modular fuel cell systems [1, 2] in hydrogen powered vehicles could lead to its emergence as a more competitive alternative in the actual market.

The hybridisation of fuel cell systems with batteries enables control over the power provided by the fuel cell [3]. Such control can lead to increased lifetime and efficiency. This increase is most notable in automotive applications. Indeed, the highly dynamic driving cycles specific to the automotive industry and severe conditions of operation lead to accelerated ageing of the fuel cell system if unrestricted. Multi-stack fuel cell (MFC) systems [4] offer another level of control which can be used to even further the advantages of hybridisation through the use of power distribution methods [5].

Early results [5] show that the MFC architecture achieves a higher efficiency than single-stack fuel cell architecture if efficiency dedicated power distributions is used. The redundancy introduced by MFC architectures can also be used for degraded mode operation in order to increase its reliability. Previous research [6] on the reliability of MFC system show that, through individual fuel cell control, the flooding and drying of the cells can be reduced. Fuel cell failure has also been tackled [7, 8]. The system still retains the ability to provide power whereas the single-fuel cell architecture cannot. This is critical in transportation applications. Moreover, MFC system can operate at a lower minimum power than single-fuel cell system if used in a cascaded, parallel or series-parallel architecture.

A previous study of the energetic behaviour of an MFC system during degraded mode operation has been conducted in [9]. It showed that, considering an appropriate sizing of the fuel cell stacks and batteries, the system could still function under degraded conditions with an increase in fuel consumption. However, this study focused on the behaviour of the fuel cell stacks and did not include the ancillaries.

The aim of this paper is to analyse the energetic behaviour of MFC systems upon the loss of one of its stack.

The first section presents the energy management problem introduced by hybrid vehicle. Two levels of energy management are introduced to account for the different levels of redundancy. The first level distributes the load between the fuel cell and the battery. The second level of energy management distributes the part of the load attributed to the fuel cell system to the different fuel cells. It is accomplished through the use of power distribution methods. Three of them are presented in Section 2. The fuel cell system model used in simulations is presented in Section 3. In Section 4, the normal and degraded operation are presented and compared. Fuel consumption results on a driving cycle obtained on the mobile laboratory of the Hydrogen Research Institute are presented along with a discussion of those results.

2 Energy management of a hybrid MFC/battery vehicle

2.1 Hybrid fuel cell/battery vehicle

The hybrid fuel cell/battery architecture and MFC/battery architectures are presented in this section.

The fuel cell/battery hybrid architecture is presented in Fig. 1.

The hybridisation of a fuel cell system and a battery pack provides a new degree of freedom. This degree of freedom enables the distribution of the load's power request between the battery and the fuel cell (FC) system. The fuel cell system presented in this paper is based on the Hydrogen Research Institute's test bench and is composed of an air breathing fuel cell stack, a hydrogen supply system and a DC–DC converter to adapt the power output. The study would yield similar results if adapted to other fuel cell system architectures.

The MFC system can replace the aforementioned fuel cell system. Multiple architectures are available for MFC systems [4]. The isolation of a failed segment or stack impacts the system differently depending on the chosen electrical architecture. Series configurations require by pass systems to isolate failed stacks and can lead to current peaks damaging the system during the reconnection of the recovered stack. Parallel and cascaded configurations do not require by pass systems and are not subject to current peaks because they provide individual current control. The parallel architecture is the one considered in this study because of its increased modularity and ability to efficiently integrate degraded mode operation capabilities. Each FC system of the MFC system is composed of a fuel cell stack and a dedicated DC–DC converter. This hybrid architecture is presented in Fig. 2.

When coupled with an MFC system, additional degrees of freedom are introduced. They can be used to distribute the load's power demand between the multiple fuel cell of the system. The multiple degrees of freedom can be decoupled in order to define two different energy management strategies:

(i) The battery/MFC system level energy management strategy that splits the power between the batteries and the MFC system.
(ii) The MFC system level energy management that distributes the power between the different fuel cells.

Energy management strategies [10] can be used to maximise efficiency and/or to minimise degradation [11, 12]. In this study, the battery/MFC system level energy management will aim at minimising degradations while the MFC system level management will focus on maximising efficiency.

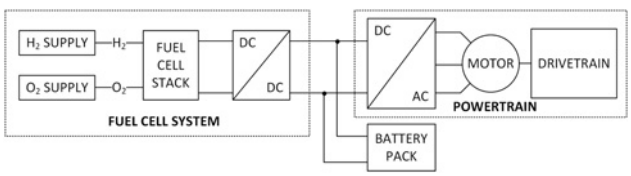

Fig. 1 *Hybrid system architecture*

IET Electr. Syst. Transp., 2016, Vol. 6, Iss. 1, pp. 3–11

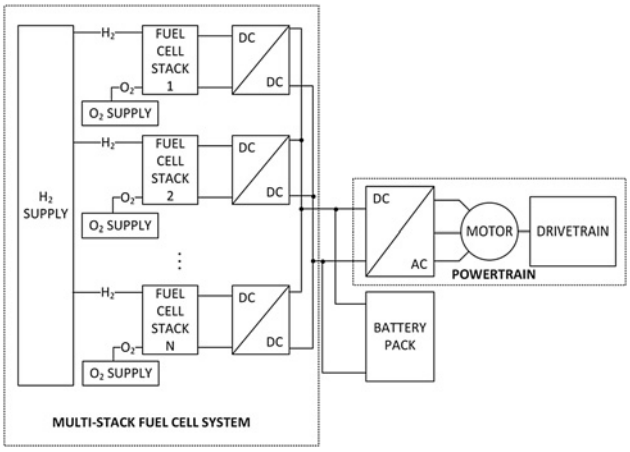

Fig. 2 *Hybrid system architecture with MFC system*

2.2 Battery/MFC system level energy management strategy

The battery/MFC system level energy management focuses on minimising the ageing of the MFC system and the battery system.

The ageing of the fuel cell systems is affected by the dynamics of the current reference or other factors like start and stop cycles, operation time, shutdown procedure or the environment. The battery's ageing is affected mainly by the depth of discharge. The following constraints have been chosen accordingly to design the vehicle level energy management strategy:

(i) The fuel cell system requires current reference with slow dynamics (maximum rate: 4 A s^{-1} [13]).
(ii) The variation of the battery state of charge (SOC) between the beginning and the end of the driving cycle must be kept between 60 and 80%.

The control of the battery SOC's variations is achieved through its regulation with a proportional corrector. The limitation of the fuel cell current dynamics is achieved through a low-pass filter and a rate limiter. The proposed strategy is presented in Fig. 3.

2.3 MFC system level energy management strategy

The MFC system level energy management strategy distributes the power demand between the different fuel cells of the system. This can be done through the use of power sharing methods designed for MFC systems [5]. Three power sharing methods will be presented in this subsection.

The input degrees of freedom are the individual fuel cell powers (P_{FC_i}). The output is the required total power output (P_{tot})

$$P_{\mathrm{tot}} = \sum_{i=1}^{N} P_{\mathrm{FC}_i} \tag{1}$$

i. *Equal distribution:* The equal distribution splits the power reference equally between the N fuel cells, that is

$$\forall i \in \{1, \ldots, N\},\ P_{\mathrm{FC}_i} = \frac{P_{\mathrm{tot}}}{N} \tag{2}$$

This distribution has an energetic behaviour close to the single-fuel cell system.

ii. *Daisy-chain algorithm:* The daisy-chain power sharing method is a sequential method. When one fuel cell cannot achieve the output, other fuel cells are used to try achieving it. If fuel cell 1 operates at maximum power

$$P_{\mathrm{FC}_2} = P_{\mathrm{tot}} - P_{1,\max} \tag{3}$$

If fuel cell 2 operates at maximum power

$$P_{\mathrm{FC}_3} = P_{\mathrm{tot}} - P_{2,\max} - P_{1,\max} \tag{4}$$

If fuel cell k operates at maximum power

$$P_{\mathrm{FC}_{k+1}} = P_{\mathrm{tot}} - \sum_{i=1}^{k} P_{i,\max} \tag{5}$$

As it is a sequential method, it requires a fuel cell order. The fuel cell order that provides the best average efficiency for the daisy-chain method is the one that ranks the fuel cells according to their average efficiency

$$\eta_{\mathrm{average}} = \frac{1}{P_{\max}} \int_{P=0}^{P_{\max}} \eta(P)\mathrm{d}P \tag{6}$$

iii. *Optimal distribution:* The optimal distribution provides the different power reference P_{FC_i} for each fuel cell in order to maximise efficiency and satisfy the total power demand. This is

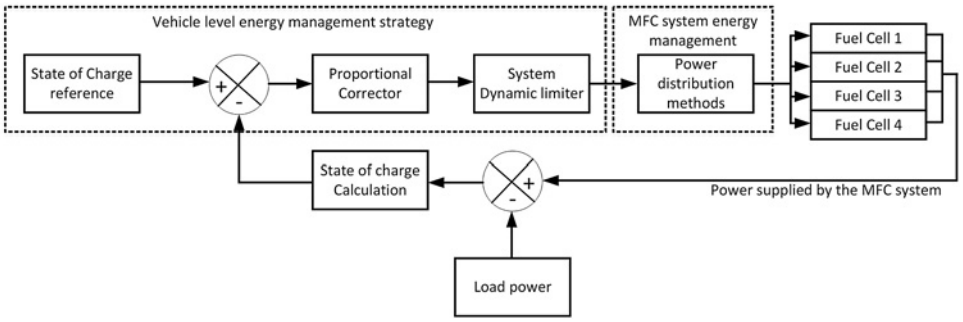

Fig. 3 *Energy management strategy*

translated into the following optimisation problem

$$F = \max_{P_{\mathrm{FC}_i}, i\in\{1..N\}} \eta(P_{\mathrm{tot}}) \tag{7}$$

$$\forall i \in \{1, \ldots, N\},\ 0 \le P_{\mathrm{FC}_i} \le P_{i,\max} \tag{8}$$

$$\sum_{i=1}^{N} P_{\mathrm{FC}_i} = P_{\mathrm{tot}} \tag{9}$$

where the efficiency of the system is

$$\eta(P_{\mathrm{tot}}) = \frac{P_{\mathrm{tot}}}{\mathrm{LHV} \cdot \mathrm{flow}(P_{\mathrm{FC}_1}, \ldots, P_{\mathrm{FC}_N})} \tag{10}$$

The optimal distribution is obtained offline and implemented online through a look-up table, whereas the other distribution can be implemented online directly.

3 Fuel cell system model

A model including the fuel cell stack and its ancillaries is required to obtain a relevant evaluation of the fuel consumption during operation and to solve the aforementioned optimisation problem. Air breathing fuel cells are usually paired with blowers and a power converter. The blowers act as the cooling system and provide the oxidant to fuel the reaction. The converter adapts the power output to meet the requirement of the application and regulates the power delivered by the fuel cell. The models chosen for the fuel cell stack, blower system, power converter and battery pack will be detailed in the following subsections.

3.1 Electrochemistry

The cell voltage, internal heat generation and consumption of reactant inside the fuel cell are based on the laws of electro-chemistry.

(i) *Potential calculation:* The static potential of the cells is calculated through (11). This equation defines the polarisation curve

$$V_{\mathrm{cell,s}} = E_n - \Delta V_{\mathrm{act}} - \Delta V_{\mathrm{conc}} - \Delta V_{\Omega} \tag{11}$$

The Nernst potential is given by [14]

$$E_{\mathrm{n}} = -\frac{\Delta H - T\Delta S}{2F} + \frac{RT_{\mathrm{FC}}}{2F} \times \ln\left(\frac{P_{\mathrm{H_2}} \times {P_{\mathrm{O_2}}}^{1/2}}{{P_0}^{3/2}}\right) \tag{12}$$

The different voltage losses are calculated through the following equations [15]

$$\Delta V_{\mathrm{act}} = K_1 \frac{RT_{\mathrm{FC}}}{F} \ln\left(\frac{j + j_{\mathrm{loss}}}{j_0}\right) \tag{13}$$

$$\Delta V_{\mathrm{conc}} = K_3 T_{\mathrm{FC}} \ln\left(1 - \frac{j}{j_{\mathrm{L}}}\right) \tag{14}$$

$$\Delta V_{\Omega} = R_{\mathrm{m}} I_{\mathrm{FC}} \tag{15}$$

$$j_0 = K_2 \frac{P_{\mathrm{O_2}}}{P_0} \exp\left(-\frac{E_c}{RT_{\mathrm{FC}}}\left(1 - \frac{T_{\mathrm{FC}}}{T_0}\right)\right) \tag{16}$$

$$R_{\mathrm{m}} = K_4 \frac{t_{\mathrm{mb}}}{b_{11} \times \Lambda_{\mathrm{mb}} - b_{12}} \exp\left(-K_5 \times \left(\frac{1}{T_0} - \frac{1}{T_{\mathrm{FC}}}\right)\right) \tag{17}$$

Multiple dynamic phenomena take place inside the fuel cell. The charging of the double layer capacity, the diffusion of gas in the gas diffusion layer or the membrane hydration have been thoroughly studied [16]. The model is to be used for energy management purposes, thus, the dynamic impact of membrane hydration on voltage will be the only phenomenon considered as it is the one with the most significant impact on energy calculations.

This phenomenon is modelled using an empiric approach. As it is a consequence of current transients, the following differential equation has been considered

$$V_{\mathrm{cell,d}} + \tau \frac{\mathrm{d}V_{\mathrm{cell,d}}}{\mathrm{d}t} = K \frac{\mathrm{d}I}{\mathrm{d}t} \tag{18}$$

The fuel cell voltage is obtained by adding the static and dynamic cell voltages and multiplying it by the number of cell. This equation is valid under the assumption that all cells work at the same operating point and are equally aged

$$V_{\mathrm{FC}} = N_{\mathrm{cell}}(V_{\mathrm{cell,s}} + V_{\mathrm{cell,d}}) \tag{19}$$

ii. *Reactant consumption:* The consumption of reactant depends on the stack current through the following equations:

$$q_{\mathrm{H_2,r}} = \frac{N_{\mathrm{cell}} I_{\mathrm{PAC}}}{2F} \tag{20}$$

$$q_{\mathrm{O_2,r}} = \frac{N_{\mathrm{cell}} I_{\mathrm{PAC}}}{4F} \tag{21}$$

iii. *Heat generation:* The electrochemical reaction is exothermic. The internal heat generation is given by

$$\Delta S_{\mathrm{q}} = N_{\mathrm{cell}} \frac{(\Delta H/2F - V_{\mathrm{cell}}) I_{\mathrm{PAC}}}{T_{\mathrm{FC}}} \tag{22}$$

3.2 Reactant supply

The model of the reactant supply subsystem presented in this paper is based on two equivalent electric circuits. The air supply subsystem is modelled as presented in Fig. 4*a*. The hydrogen supply subsystem is modelled as presented in Fig. 4*b*.

(i) *Air supply:* The flow of air between the inlet and outlet of the cathode is given by

$$q_{\mathrm{air,in}} = \frac{P_{\mathrm{air,out}} - P_{\mathrm{air}}}{R_{\mathrm{air}}} \tag{23}$$

$$q_{\mathrm{air}} = q_{\mathrm{air,in}} - x_{\mathrm{O_2}} \cdot q_{\mathrm{O_2,r}} \tag{24}$$

The pressure in the space confined between the blowers and the cathodic chamber is based on the ideal gas law

$$P_{\mathrm{air}} = \frac{1}{C_{\mathrm{AIR}}} \int (q_{\mathrm{air}} - q_{\mathrm{air,fan}})\mathrm{d}t \quad \text{with} \quad C_{\mathrm{AIR}} = \frac{V_{\mathrm{mol,air}} \times V_{\mathrm{fan}}}{RT_{\mathrm{FC}}} \tag{25}$$

The blowers are located at the cathode outlet and draw up air into it. A complete model of the blower subsystem is detailed in Section 3.4.

ii. *Hydrogen supply:* The pressure loss between the hydrogen tank and the anode inlet is obtained through the following equation:

$$q_{\mathrm{H_2,in}} = \frac{P_{\mathrm{H_2 in}} - P_{\mathrm{H_2}}}{R_{\mathrm{H_2}}} \tag{26}$$

IET Electr. Syst. Transp., 2016, Vol. 6, Iss. 1, pp. 3–11

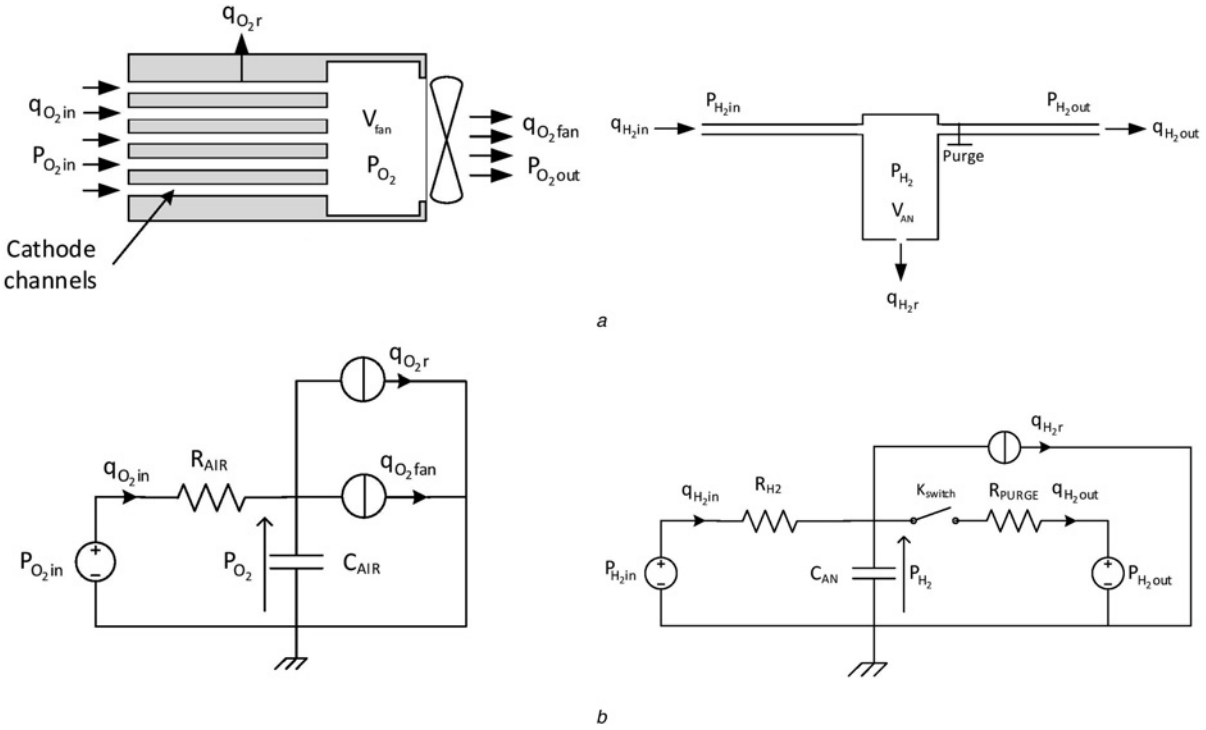

Fig. 4 *Fluidic system and associated electric circuit equivalent for the reactant supply subsystems*

a Air supply architecture
b Hydrogen supply architecture

The pressure in the anodic chamber is obtained through the following equation

$$P_{H_2} = \frac{1}{C_{AN}} \int (q_{H_2in} - q_{H_2c}) dt$$
$$\text{with } C_{AN} = \frac{V_{mol} \times V_{AN}}{RT_{FC}} \tag{27}$$

The flow of hydrogen at the anode inlet $q_{H_2}c$ is the sum of the flow consumed by the reaction and the flow expelled through the purge

$$q_{H_2c} = q_{H_2out} + q_{H_2,r} \tag{28}$$

The dead-end mode operation of fuel cells requires a purge in order to evacuate excess water. The flow of hydrogen evacuated during the purge depends on the geometry of the purge orifice, the pressure difference between the anodic chamber and the outlet as well as the state of the purging valve

$$q_{H_2,out} = K_{purge} \frac{P_{H_2} - P_{H_2,out}}{R_{purge}} \tag{29}$$

3.3 Thermal behaviour

The temperature of the fuel cell is affected by multiple phenomena. Its calculation will consider the forced convection, free convection and internal heat generation as the heat transfer sources. The internal heat generation is caused by the electrochemical reaction and has been covered in Section 3.1. The forced and free convection are covered in this subsection. The considered fuel cell temperature is the mean temperature of the stack.

(i) *Free convection:* The free convection on the stack's external surface is obtained through the following equation

$$q_{conv,free} = h_{free} A (T_{FC} - T_{Air}) \tag{30}$$

(ii) *Forced convection:* The model presented in this section originates from [17] and was used with air breathing fuel cell systems [18]. The heat transfer rate is calculated with the following formula

$$q_{conv,forced} = \bar{h} A_t \eta_{therm} \theta_{b,lm} \tag{31}$$

The variables $\bar{h}$ and $\theta_{b,lm}$ are highly dependent on the air flow considered for the convection. Those dependencies are detailed in [18]. The total convection heat exchange is the sum of the free and forced convections

$$q_{conv} = q_{conv,free} + q_{conv,forced} \tag{32}$$

3.4 Blower subsystem

The blower (Fig. 5) is composed of a DC electrical motor power rotating fans that evacuates air out of the fuel cell stack.

The behaviour of the current in the windings of the motor depends on an internal resistance and an internal inductance through the

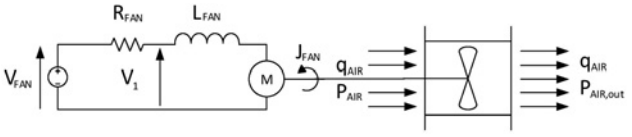

Fig. 5 *Chosen model of the blower subsystem*

following equations

$$V_1 = V_{FAN} - R_{FAN} I_{FAN} \tag{33}$$

$$I_{FAN} = \frac{1}{L_{FAN}} \int (V_1 - E) \mathrm{d}t \tag{34}$$

The electromechanical conversion is described by (35) and (36). Iron and mechanic losses are subtracted to the electromechanical torque

$$E = k\Omega \tag{35}$$

$$T_m = kI_{FAN} - T_{loss} \tag{36}$$

The behaviour of the motor axis and the fan blades is dependent on their total inertia J

$$\Omega = \frac{1}{J_{FAN}} \int (T_M - T_{aero}) \mathrm{d}t \tag{37}$$

Conversion of the blades rotation into air flow is given by (38). Drag forces lead to a resistive torque on the motor's axis

$$q_{air} = \eta_{aero} k_{aero} \Omega \tag{38}$$

$$\begin{aligned} T_{aero} &= N_b \int_{r=R_0}^{R_b} \left(\frac{1}{2} \rho_{air} C_d e_b (r\Omega \cos\theta)^2 \right) \cdot r \mathrm{d}r \\ &= N_b \left(\frac{1}{8} \rho_{air} C_d e_b (R_b^4 - R_0^4)(\Omega \cos\theta)^2 \right) \end{aligned} \tag{39}$$

3.5 DC–DC converters

Fuel cells are often coupled to scale-up converters because they are low-voltage high-current power sources [19]. Using a dedicated inductance, the output current control is performed in the converter

$$I_{conv} = \frac{1}{L_{conv}} \int (V_{bus} - V_{conv}) - I_{loss} \mathrm{d}t \tag{40}$$

The voltage step-up stage is modelled by (41) and (42) which correspond to that of a boost converter

$$V_{conv} = \frac{1}{1-\alpha} V_{FC} \tag{41}$$

$$I_{FC} = \frac{1}{1-\alpha} I_{conv} \tag{42}$$

3.6 Battery model

The battery is modelled as a constant voltage source coupled to a resistance. The voltage source represents the open circuit voltage and the resistance models the internal resistance of the battery [20]. The output voltage is dependent on current and is calculated through the following equation

$$V_{bat} = \mathrm{OCV} - R_{bat} I_{bat} \tag{43}$$

The state of charge of the battery is calculated through the following equation

$$\mathrm{SOC} = \frac{1}{C_{bat}} \int I_{bat} \mathrm{d}t \tag{44}$$

where C_{bat} is the capacity of the battery.

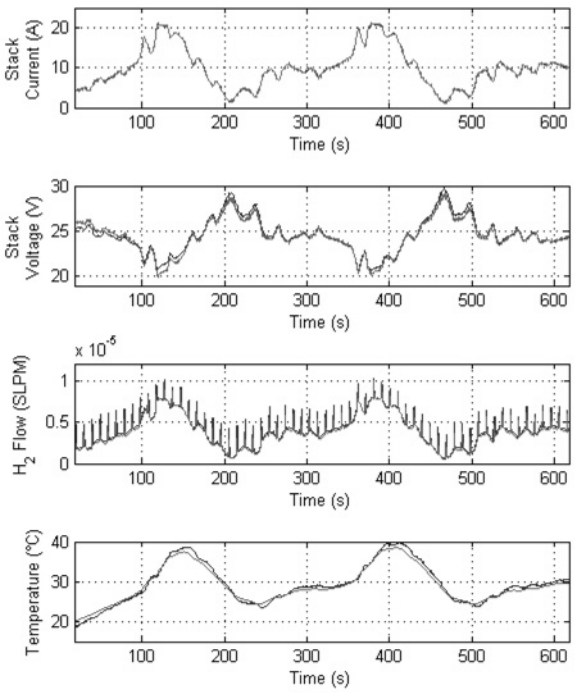

Fig. 6 *Comparison of the simulation results and the experimental data acquisition*

3.7 Model validation

The model has been validated with a dynamic current profile. Fig. 6 presents the current reference, stack voltage, hydrogen flow and temperature.

The black curves represent experimental results. The grey curves represent simulation results. Overall, the different curves show little error (up to 4% for the voltage).

4 Normal and degraded mode operation

The multi-stack parallel architecture provides multiple advantages when compared with the series architecture. One of these is enabling degraded mode operation when part of the system fails. In this section, fuel consumption in the normal and degraded operation will be evaluated and compared.

4.1 Problem formulation

Single-stack fuel cell systems require multiple auxiliaries in order to function. The failure of any of them will lead to the failure of the whole system. For MFC system, the other FC systems can still achieve part of the power output in order to keep on operating. If sized accordingly, the system will be able to keep operating without restricting the user. It will however lead to repercussions on fuel consumption. A low speed vehicle application is considered in this study. The mobile laboratory of the Hydrogen Research Institute (NEMO) has been used to obtain a driving profile in real driving conditions. It is a hybrid fuel cell/battery vehicle with on board instrumentation (Fig. 7*a*). The chosen driving cycle and corresponding power profile are presented in Fig. 7*b*.

4.2 System description

The parameters of the fuel cell model have been fitted to the MFC test bench of the Hydrogen Research Institute. It is composed of four 400 W FC systems (manufacturer: Horizon, model: H500) and a 72 V battery system. Each fuel cell system includes a

IET Electr. Syst. Transp., 2016, Vol. 6, Iss. 1, pp. 3–11

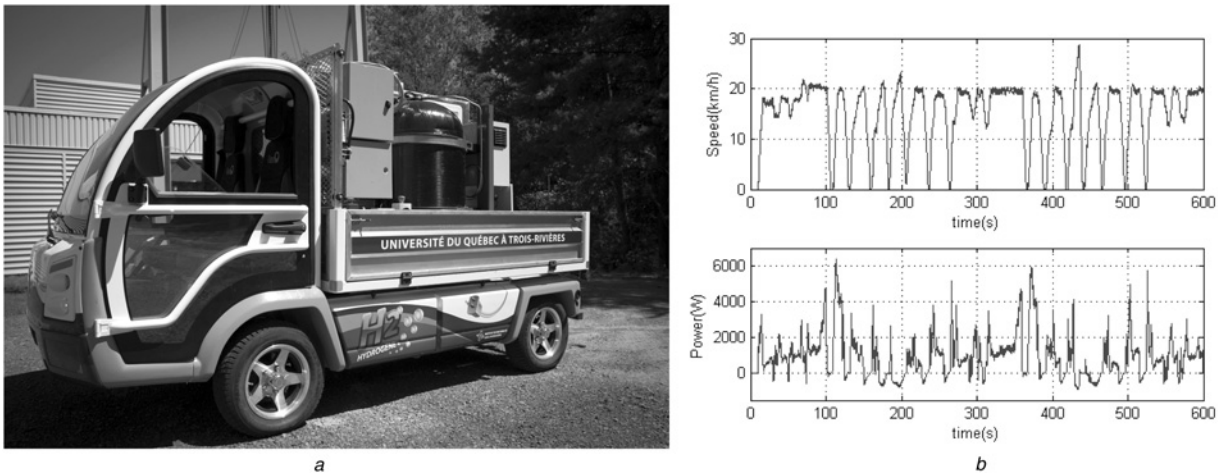

Fig. 7 *Driving cycle acquired on a test vehicle*

a mobile laboratory NEMO
b Driving cycle and power profile

dedicated DC–DC converter for individual power control. The steady-state efficiency curves of the different FC systems are presented in Fig. 8. The fuel cells exhibit different behaviours in terms of efficiency because of different ageing and because of a manufacturing process that does not guaranty identical behaviours.

4.2.1 Complete system: The effect of the MFC system level energy management on the MFC system efficiency is evaluated over the complete power range of the system. The optimal power distribution resulting from the optimisation problem presented in Section 2 is shown in Fig. 9*a*.

The optimal and daisy-chain distribution clearly offer an advantage over the equal distribution in the lower power range. Nevertheless, in 800–1600 W power range, the equal distribution provides results similar to those of the optimal distribution. Finally, the daisy-chain distribution falls behind after 800 W.

4.2.2 System without fuel cell 3: Degraded mode operation will be simulated by removing the third fuel cell (the less efficient one) from the system. The optimisation process is then conducted to obtain the optimal power distribution for this system (Fig. 9*b*) and the comparison of the different power sharing methods (Fig. 9*d*).

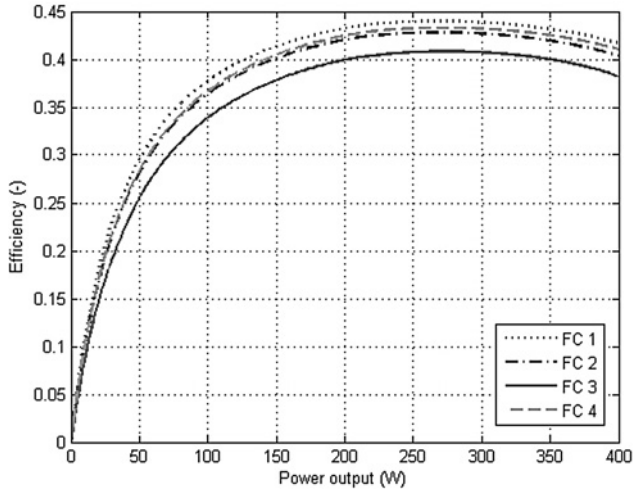

Fig. 8 *Efficiency of the four fuel cell systems*

The results are similar to that of the complete system with the exception that the daisy-chain distribution is now the less efficient distribution above 400 W (one-third of the rated power of the system). The system still retain the ability to provide power whereas the single-fuel cell architecture cannot.

4.3 Simulation results

The aforementioned driving cycle is linked to a corresponding power profile. That power profile is scaled down in order to reduce the average power to two-third of the system's rated power (1600 W). The resulting power profile is presented in Fig. 10*a*. The battery/MFC system level energy management strategy is applied to that power profile and depending on the scenario evaluated (normal or degraded mode operation) a new power profile is generated for the MFC system (plain and dashed curves in Fig. 10*a*). The resulting effect of this power profile on the SOC's variation is presented in Fig. 10*b* and respects the constraints introduced in Section 3. Considering that the power profile imposed to the MFC system for the normal and degraded operation does not vary by a large margin (Fig. 10*a*), the power provided by the batteries remains similar. Therefore, the batteries are not subject to critical degradations due to high power peaks. However, these results are highly dependent on the system's sizing.

The fuel consumption results are presented in Table 1 for the two scenarios and additional scenarios in which the removed fuel cell system differs.

4.4 Discussion

The system has been sized so that the average power required by the load is two-third of the rated power of the MFC system. Thus, even with the loss of one stack the system can still operate as it did before. The fuel consumption during normal and degraded mode operation presented in Table 1 do not differ by a large margin. There is however a small difference depending on the removed fuel cell. The difference depends on the performance of that fuel cell compared with the others. Thus, the loss of a fuel cell with a higher efficiency like the first fuel cell will increase the hydrogen consumption of the system. The difference between the scenarios in which the first and the third fuel cell are removed results in a difference in hydrogen consumption of 1.3% in favour of the later.

The loss of one stack does not lead to substantial change in the simulation results. The main factor ruling the changes is maximum power rating of three FC systems. With 1.2 kW the

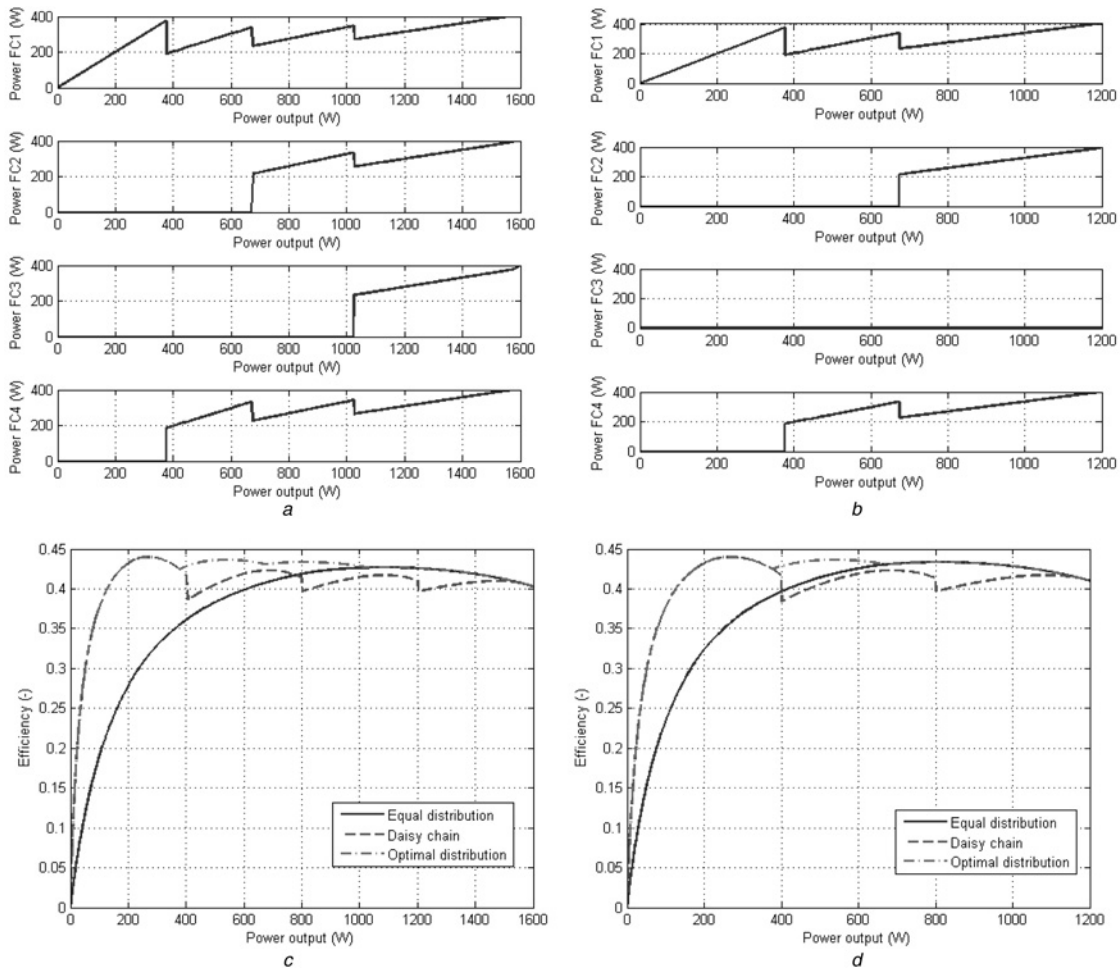

Fig. 9 *Comparison of the complete system and the system without fuel cell 3*

a Optimal power distribution for the complete system
b Optimal power distribution for the system without fuel cell 3
c Efficiency comparison of the different distribution method for the complete system
d Efficiency comparison of the different distribution method for the system without fuel cell 3

fuel cell power reference cannot remain the same as with four FCs. The change in power reference leads to change in the evolution of the SOC during the cycle. However, the SOC remains within acceptable limits. With only three FCs, the fuel cells will work closer to their maximum power rating and could thus age more rapidly.

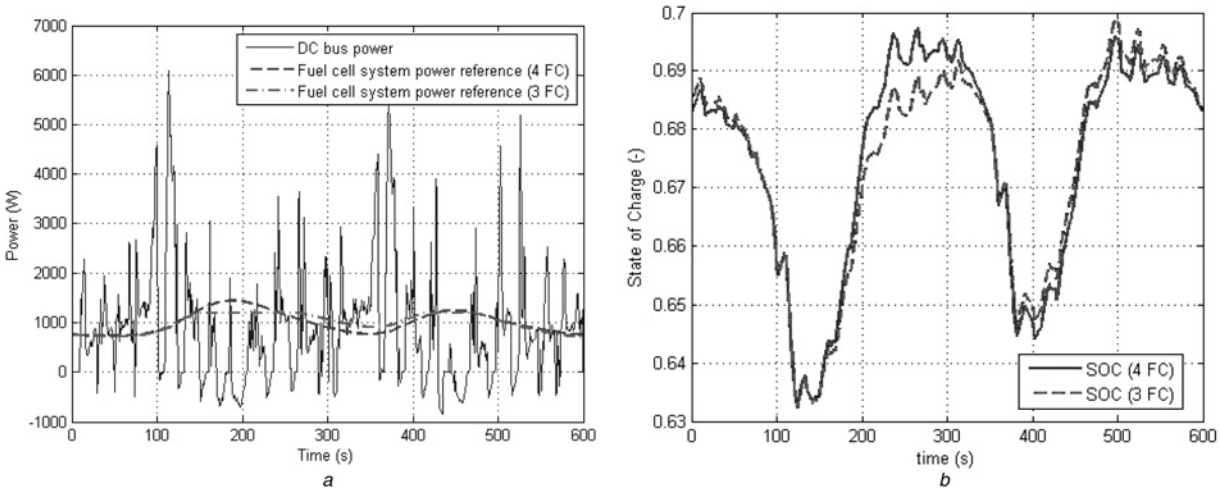

Fig. 10 *Simulation results*

a Power profiles for the different scenario
b Evolution of the State of Charge for the different scenario

IET Electr. Syst. Transp., 2016, Vol. 6, Iss. 1, pp. 3–11

Table 1 Fuel consumption results (hydrogen mass)

	Normal operation	Degraded mode operation without FC 1	Degraded mode operation without FC 2	Degraded mode operation without FC 3	Degraded mode operation without FC 4
equal distribution	19.61 g	19.86 g	19.74 g	19.56 g	19.82 g
daisy chain	19.93 g	20.06 g	19.90 g	19.80 g	20.00 g
optimal distribution	19.40 g	19.85 g	19.72 g	19.57 g	19.80 g

5 Conclusions

The results of this study highlight the interest of MFC system for degraded mode operation. The system can still function and complete a driving cycle even when one stack is removed from the system. The only requirement being that a reconfiguration of the system in order to use the optimal power distribution has to be performed. However, working without the complete system involves higher fuel consumption when the most efficient fuel cells are lost because the efficiency is reduced. The fuel consumption results during degraded mode operation depend on which fuel cell is isolated.

The sizing of the system is an important factor. It impacts the capabilities in degraded mode operation. Higher peak power for the MFC system could lead to better capabilities in degraded mode such as allowing the possibility of a second stack failing. However, it could also lead to a reduced sizing of the battery, which could lead in turn to high current damaging it during degraded operation. The sizing was constant in this study but should be variable in further studies to account for other optimisation such as durability and operation cost optimisations. This could lead to less advantageous system sizings which could lead to different results.

The loss of one stack has been considered in this study. However, depending on the fault emerging on the fuel cell stacks they could be used at a reduced power level before being turned off. Furthermore, the loss of more than one stack would impose a reconfiguration of the maximum acceleration and speed of the vehicles which has not been covered in this study either and shall be addressed in future works.

6 References

1 Williams, M.: 'Fuel cells and the world energy future'. Power Engineering Society Summer Meeting Conf. Proc., Vancouver, Canada, 2001, p. 725

2 Le, T.: 'Fuel cells: the epidemic of the future'. Proc. of Electrical Insulation Conf. and Electrical Manufacturing and Coil Winding Technology Conf., Indianapolis, USA, 2003, pp. 505–510

3 Yu, X., Starke, M., Tolbert, L., *et al.*: 'Fuel cell power conditioning for electric power applications: a summary', *IET Electr. Power Appl.*, 2007, **1**, (5), pp. 643–656

4 Marx, N., Boulon, L., Gustin, F., *et al.*: 'A review of multi-stack and modular fuel cell systems: interests, application areas and on-going research activities', *Int. J. Hydrog. Energy*, 2014, **39**, (23), pp. 12101–12111

5 Garcia, J.E., Herrera, D.F., Boulon, L., *et al.*: 'Power sharing for efficiency optimisation into a multi fuel cell system'. Int. Symp. on Industrial Electronics Istanbul, Turkey, 2014, pp. 218–223

6 Frappe, E., De Bernardinis, A., Coquery, G., *et al.*: 'Corrective action with power converter for faulty multiple fuel cells generator used in transportation'. Vehicle Power and Propulsion Conf., Lille, France, 2010, pp. 1–6

7 De Bernardinis, A., Coquery, G.: 'First approach for a fault tolerant power converter interface for multi-stack PEM fuel cell generator in transportation systems'. Int. Power Electronics and Motion Control Conf., Poznan, Poland, 2008, pp. 2192–2199

8 Candusso, D., De Bernardinis, A., Péra, M.-C., *et al.*: 'Fuel cell operation under degraded working modes and study of diode by-pass circuit dedicated to multi-stack association', *Energy Convers. Manage.*, 2008, **49**, (4), pp. 880–895

9 Toquica Cardenas, D.C., Marx, N., Boulon, L., *et al.*: 'Degraded mode operation of multi-stack fuel cell systems'. Vehicle Power Propulsion Conf., Coimbra, Portugal, 2014, pp. 1–6

10 Allègre, A.-L., Trigui, R., Bouscayrol, A.: 'Flexible real-time control of a hybrid energy storage system for electric vehicles', *IET Electr. Syst. Transp.*, 2013, **3**, (3), pp. 79–85

11 Panigrahi, S.P., Panigrahi, B.K., Samanta, C.: 'Genetic-based bacteria foraging to optimise energy management of hybrid electric vehicles', *IET Electr. Syst. Transp.*, 2014, **4**, (3), pp. 53–61

12 Pereirinha, P.J.G., Trovão, J.a.P.F.: 'Control scheme for hybridised electric vehicles with an online power follower management strategy', *IET Electr. Syst. Transp.*, 2015, **5**, (1), pp. 12–23

13 Thounthong, P., Raël, S., Davat, B.: 'Energy management of fuel cell/battery/supercapacitor hybrid power source for vehicle applications', *J. Power Sources*, 2009, **193**, (1), pp. 376–385

14 Barbir, F.: 'PEM fuel cells theory and practice' (Academic Press, Waltham, 2013, 1st edn.)

15 Springer, T.E.: 'Polymer electrolyte fuel cell model', *J. Electrochem. Soc.*, 1991, **138**, (8), pp. 2334–2342

16 Ceraolo, M., Miulli, C., Pozio, A.: 'Modelling static and dynamic behaviour of proton exchange membrane fuel cells on the basis of electro-chemical description', *J. Power Sources*, 2003, **113**, (1), pp. 131–144

17 Incropera, F.: 'Fundamentals of heat and mass transfer' (John Wiley and Sons, New York, 2002, 5th edn.)

18 Higuita Cano, M., Kelouwani, S., Agbossou, K., *et al.*: 'Free air breathing proton exchange membrane fuel cell: thermal behavior characterization near freezing temperature', *J. Power Sources*, 2014, **246**, pp. 650–658

19 Ortega, M., Valverde, M., Jurado, F.: 'Novel topology for DC/DC unidirectional converter for fuel cell', *IET Power Electron.*, 2014, **7**, (3), pp. 681–691

20 Chen, S., Gooi, H., Xia, N., *et al.*: 'Modelling of lithium-ion battery for online energy management systems', *IET Electr. Syst. Transp.*, 2012, **2**, (4), pp. 202–210